scientific reports

Check for updates

OPEN

$1,25(OH)_2D_3$ inhibits ferroptosis in nucleus pulposus cells via VDR signaling to mitigate lumbar intervertebral disc degeneration

Qiang Li[1,3], Jing Peng[2,3] & Fan Ding[1]✉

Lumbar intervertebral disc degeneration (LIDD) serves as a principal contributor to low back pain, a condition that poses considerable global health and socioeconomic challenges. Recent studies have emphasized the significance of ferroptosis, an iron-dependent mechanism of programmed cell death, in the degeneration of nucleus pulposus cells (NPCs). This research examines the protective role of 1,25-dihydroxyvitamin D_3 [$1,25(OH)_2D_3$], the active metabolite of Vitamin D (VD), in LIDD through the modulation of ferroptosis. The results indicate that $1,25(OH)_2D_3$ significantly inhibits ferroptosis in NPCs through the reduction of lipid peroxidation, restoration of glutathione levels, and enhancement of antioxidant defenses. $1,25(OH)_2D_3$ exerts its effects by activating the VD receptor (VDR) signaling pathway, which regulates important ferroptosis-associated molecules, including glutathione peroxidase 4 (GPX4) and solute carrier family 7 member 11 (SLC7A11). The findings indicate the therapeutic potential of $1,25(OH)_2D_3$ in alleviating LIDD, presenting a new strategy to inhibit ferroptosis and maintain intervertebral disc function.

Keywords Lumbar intervertebral disc degeneration, $1,25(OH)_2D_3$, Ferroptosis, Nucleus pulposus cells, Vitamin D receptor

Low back pain represents an increasingly significant global health issue, affecting more than 80% of the worldwide population and resulting in considerable social and economic costs[1,2]. Intervertebral disc degeneration significantly contributes to low back pain[3]. LIDD includes various structural and tissue changes, such as reduced disc height, nucleus pulposus fissures, tears in the annulus fibrosus, calcification of the cartilaginous endplate, and altered extracellular matrix metabolism[4,5]. The precise mechanisms underlying LIDD remain unclear. Nonetheless, it is generally accepted that LIDD is exacerbated by the depletion of NPCs and the degradation of the extracellular matrix (ECM)[5]. NPCs are integral to the synthesis and degradation of the ECM, functioning as crucial elements of the intervertebral disc, which is vital for maintaining its structural integrity and physiological functions. The decline and dysfunction of NPCs are significant factors in the progression of LIDD[6]. Consequently, investigating NPCs to clarify the pathogenesis of LIDD holds considerable clinical significance[7]. Previous studies indicate that the factors of disc degeneration could be associated with apoptosis, as a reduction in cell numbers leads to decreased ECM protein production and disruptions in cellular energy metabolism and other physiological functions[8]. Treatment for LIDD primarily focuses on preventing cell loss due to programmed or regulated cell death. Recent studies indicate that various forms of cell death, including apoptosis, pyroptosis, necroptosis, autophagy and ferroptosis, contribute to the progression of LIDD, offering new potential treatment strategies[9].

Ferroptosis, introduced in 2012 as a distinct form of programmed cell death, is characterized by its dependence on iron and a notable accumulation of lipid reactive oxygen species (ROS)[10]. It can be morphologically and biochemically differentiated from apoptosis, necrosis, autophagy-dependent cell death, and pyroptosis[11]. Ferroptosis is linked to the pathologies of various diseases, including cancer, stroke, cerebral hemorrhage, traumatic brain injury, ischemia-reperfusion injury, and neurodegenerative disorders such as Alzheimer's and Parkinson's[12]. Morphologically, ferroptosis is marked by the initial maintenance of cell membrane integrity, lipid peroxidation in cell membranes, mitochondrial alterations (such as shrinkage, reduced mitochondrial

[1]Department of Spine Surgery, Wuhan Puren Hospital, Wuhan University of Science and Technology, Benxi Rd. 1#, Wuhan 430000, Hubei, China. [2]Department of Orthopedics, The Third Affiliated Hospital of Southern Medical University, No. 183, Zhongshan Road West, Guangzhou 510630, China. [3]Qiang Li and Jing Peng contributed equally to this work. ✉email: 307185039@qq.com

cristae, and outer membrane rupture), absence of chromatin condensation, cytosolic vesiculation, and decrease in cell volume or atrophy[11,13]. Extensive research indicates a significant relationship between ferroptosis and LIDD, underscoring the potential for effective therapeutic interventions in the control of LIDD[12,14,15]. Studies on disc degeneration indicate that ferroptosis inhibitors, such as ferrostatin-1 and deferoxamine, can reduce degeneration in a tert-butyl hydroperoxide (TBHP)-induced rat model. Moreover, ferroptosis inducers TBHP and RSL3 exhibit similar effects on cell death in AFCs and NPCs, which can be inhibited by ferroptosis inhibitors, underscoring the importance of ferroptosis in the mechanism of LIDD[15].

VD plays a crucial role in the regulation of serum calcium and phosphorus levels, existing primarily in two forms: D2 and D3[16]. Vitamin D3 (VD3), also known as cholecalciferol, is synthesized from 7-dehydrocholesterol in the skin upon exposure to UV radiation or acquired through the consumption of animal-derived foods. VD3 is converted into its active form, $1,25(OH)_2D_3$, through a two-step hydroxylation process[17]. In addition to its traditional function in calcium balance, VD influences cell growth, differentiation, and programmed cell death[18]. $1,25(OH)_2D_3$ functions as an antioxidant, potentially reducing ferroptosis caused by oxidative stress through the regulation of intracellular glutathione (GSH) and superoxide dismutase (SOD)[19]. Additionally, various clinical studies indicate that a deficiency in VD may accelerate the progression of LIDD and increase the risk of lumbar disc herniation[20,21]. Conversely, VD supplementation may mitigate the degradation process and reduce the incidence of low back discomfort[22]. $1,25(OH)_2D_3$ exerts beneficial effects on LIDD by reducing inflammation, oxidative stress, and NPC apoptosis, in addition to delaying NPC aging[23]. The VDR is essential for the biological effects of $1,25(OH)_2D_3$, as it is commonly found in intervertebral disc cells and associated with disc degeneration[24]. Variations in the *Vdr* gene, specifically *TaqI (rs731236)*, *FokI (rs2228570)*, and *ApaI (rs7975232)*, are linked to an increased risk of LIDD[25,26].

Ferroptosis plays a significant role in the advancement of LIDD, and $1,25(OH)_2D_3$, a form of VD, may inhibit this mechanism. This research examines the ability of $1,25(OH)_2D_3$ to reduce LIDD by suppressing ferroptosis in NPCs via VDR, with the goal of uncovering novel preventive strategies for LIDD.

Materials and methods

Cell culture and maintenance

Rat-derived NPCs, selected for their relevance in lumbar disc studies, were obtained from SAIBAIKANG Biosciences, Shanghai. Authenticated and mycoplasma-free, these cells were initially thawed at 37 °C and cultured in a medium supplemented with 10% foetal bovine serum (FBS). The cells were cultivated in T25 flasks within a CO_2 incubator under conditions optimal for NPC growth. Cells were passaged when confluence exceeded 85%, including washing with phosphate-buffered saline (PBS) and detachment using trypsin-EDTA. Cell growth was monitored using an inverted microscope. For long-term preservation, cells were cryopreserved in a solution of 90% FBS and 10% dimethyl sulfoxide (DMSO), following a controlled-rate freezing protocol. The cells were initially stored at -80 °C and transferred to a liquid nitrogen tank.

Cell viability assessment with CCK-8

Log-phase NPCs were produced as a single-cell suspension at a concentration of 1×10^5 cells/mL and plated into 96-well plates at 10,000 cells per well. After a 24 h incubation at 37 °C in a 5% CO_2 environment for cell adhesion, the media were substituted with new medium containing different doses of $1,25(OH)_2D_3$ or control solutions, based on initial dose-response investigations. For viability measurement, 10 µL of CCK-8 solution (Beyotime Institute of Biotechnology) was applied to each well and incubated for 2 h to facilitate the colorimetric reaction. The absorbance at 450 nm was quantified in a microplate reader (Diatek Instruments), with wells containing only the medium serving as blank controls. Viability was assessed by subtracting baseline measurements from experimental and control wells, with triplicates performed for precision and repeatability. Rat NPCs were treated with varying concentrations of $1,25(OH)_2D_3$ (0, 0.01, 0.1, 1, 10, 100, and 1000 nmol/L) for periods of 6, 12, 24, and 48 h. The CCK8 test was utilised to assess cell viability.

Evaluation of inducer and biochemical marker of ferroptosis

Erastin (a specific inducer of ferroptosis) was employed to simulate an in vivo ferroptosis environment and to initiate ferroptosis in NPCs[27–29]. The study had four groups: control, $1,25(OH)_2D_3$, Erastin and $1,25(OH)_2D_3$+Erastin. The Erastin group was administered 10 µmol/L Erastin for a period of 24 h. The $1,25(OH)_2D_3$+Erastin group consisted of NPCs that underwent pre-treatment with 10 nmol/L $1,25(OH)_2D_3$ for 48 h, followed by a 24 h treatment with 10 µmol/L Erastin.

Following treatment, cells (2×10^5 per well) were grown on 6-well plates for 48 h. lactate dehydrogenase (LDH) activity was assessed using supernatants obtained from centrifugation (2000 g, 4 °C, 10 min) and examined with an LDH assay kit (Jiancheng Bioengineering, Cat. No. A020-2) from Jiancheng Bioengineering Institute. Intracellular levels of MDA, SOD, and GSH were determined after particular sample preparation protocols. Cultured cells were initially rinsed twice with pre-cooled PBS to eliminate leftover media and contaminants. Cells were subsequently lysed using a suitable lysis solution including protease and phosphatase inhibitors to avert protein breakdown and maintain enzymatic activity. The lysates underwent ultrasonication on ice (200 W power, 10 s on, 10 s off, repeated 5 times) to achieve complete cell rupture while avoiding protein denaturation. Subsequent to ultrasonication, the samples underwent centrifugation at 12,000 g for 10 min at 4 °C to eliminate cellular debris. The supernatant was collected and promptly utilised for MDA, SOD, and GSH measurement or stored in aliquots at -80 °C to prevent freeze-thaw cycles. The processed samples yielded precise assessments of intracellular oxidative stress indicators. The protein concentration was quantified by a BCA protein assay kit (Aspen Biological, Cat. No. AS1086) for normalisation purposes. The MDA content (Jiancheng Bioengineering, Cat. No. A003-1), SOD activity (Jiancheng Bioengineering, Cat. No. A001-3), and total GSH levels (Jiancheng

Bioengineering, Cat. No. A061-1) were measured using specific test kits from Jiancheng Bioengineering Institute, adhering to the manufacturer's instructions.

Flow cytometry for ROS detection

Flow cytometry was utilised for the quantification of intracellular ROS. Subsequent to trypsinization and centrifugation, cells were stained with DCFH-DA (a fluorogenic dye sensitive to ROS). Following 20-minute incubation at 37 °C with periodic inversion for uniform dye distribution, cells were washed thrice with serum-free media to eliminate excess dye and subsequently resuspended for analysis. Flow cytometric analysis was performed utilising a BD flow cytometer equipped with a 488 nm excitation and 525 nm emission filter. Stained and unstained controls were incorporated for calibration purposes. Fluorescence intensities, reflecting ROS levels, were quantified in triplicate. Data capture and analysis were conducted utilising cytometry software to assess oxidative stress levels in reaction to various treatments.

Quantitative assessment of gene expression via RT-qPCR

RNA was extracted from cells using TRIzol-based TRIpure reagent (ELK Biotechnology, Cat. No. EP031), which involved chloroform-induced phase separation and isopropanol precipitation. The purified RNA was converted to cDNA using the EntiLink™ 1st Strand cDNA Synthesis Super Mix (ELK Biotechnology, Cat. No. Equation 031). Quantitative PCR was performed using a QuantStudio 6 Flex Real-Time PCR System with EnTurbo™ SYBR Green PCR SuperMix (ELK Biotechnology, Cat. No. Equation 001). The protocol included initial denaturation, 40 amplification cycles, and melt curve analysis for product verification. Gene expression was analyzed using the comparative ΔΔCT method, normalising the expression of R-*SLC7A11*, R-*SLC40A1*, R-*VDR*, and R-*GPX4* to R-*β-actin* (R denotes rat). The primer sequences listed in Supplementary Material 1 Table S1 were designed to span exon-exon junctions to avoid amplification of genomic DNA.

Western blot analysis

For Western Blot examination, adherent cells were initially washed twice with ice-cold PBS to eliminate residual medium and debris. Cells were subsequently lysed with RIPA lysis buffer augmented with protease and phosphatase inhibitors to avert protein breakdown and dephosphorylation. The lysates were incubated on ice for 30 min, with moderate vortexing every 10 min to improve lysis efficiency. Subsequently, the lysates were centrifuged at 12,000 g for 15 min at 4 °C, and the resultant supernatant was obtained for protein quantification utilising a BCA protein assay kit. Identical quantities of protein were applied to SDS-PAGE gels for separation and subsequently transferred to polyvinylidene difluoride (PVDF) membranes. The membranes were incubated with 5% non-fat milk or bovine serum albumin (BSA) in Tris-buffered saline with Tween-20 (TBST) for 1 h at ambient temperature to inhibit non-specific antibody binding. Subsequent to blocking, the membranes were incubated overnight at 4 °C with primary antibodies (Supplementary Material 1 Table S2) diluted in TBST with 1% blocking buffer. On the following day, the membranes underwent three washes with TBST and were subsequently incubated with horseradish peroxidase (HRP)-conjugated secondary antibodies (Supplementary Material 1 Table S3) for 30 min at ambient temperature. Subsequent washes allowed for the visualisation of protein bands via an enhanced chemiluminescence (ECL) detection kit, followed by imaging on X-ray film. Band intensities were quantified by AlphaEaseFC software and normalised against a housekeeping protein to ensure precision. To confirm antibody specificity, membranes were subjected to mild stripping with a buffer, subsequently re-blocked, and re-probed with other antibodies as required.

Transmission electron microscopy for mitochondrial morphology

NPCs were fixed in an electron microscopy fixation solution (Catalog no. AS1063, Wuhan Aspen Biotechnology) at 4 °C overnight. Following fixation, samples were washed four times with PBS (15 min per wash) to remove residual fixative. Post-fixation was performed using a 1% osmium tetroxide solution prepared in 0.1 M phosphate-buffered saline (PBS, pH 7.4) at room temperature (20 °C) for 2 h, followed by another four PBS washes (15 min each). Samples were then sequentially dehydrated in graded ethanol solutions at concentrations of 50%, 70%, 80%, 90%, 95%, 100%, and a second 100% ethanol, with each step lasting 15 min. This was followed by two rounds of treatment with reagent-grade 100% acetone for 15 min each to facilitate resin infiltration. For infiltration, samples were immersed in acetone: embedding agent mixtures at volume ratios of 2:1 for 1 h, then 1:1 for 1 h (this step was omitted for cell samples), and finally 1:2 for 4 h, followed by two incubations in pure embedding resin (each for 24 h). The resin was polymerized at 65 °C for 48 h. Ultrathin sections (approximately 70 nm thick) were prepared using a Leica EM UC7 ultramicrotome. For staining, sections were incubated in a 2% uranyl acetate solution for 10 min, washed thoroughly with distilled water, and then stained with a 0.4% lead citrate solution for 10 min before a final rinse. Finally, the sections were examined using a FEI TECNAI G2 SPIRIT transmission electron microscope, and images were acquired for mitochondrial morphology analysis.

VDR gene Silencing

To validate that $1,25(OH)_2D_3$ promotes NPC survival via VDR activation, three siRNA sequences (*si-VDR-1*, *si-VDR-2* and *si-VDR-3*) were designed using Primer5 and synthesized by RiboBio Co., Ltd. (Guangzhou, China) to silence the VDR gene in NPCs, with a non-targeting control (si-Control) included (Supplementary Material 1 Table S4). Bioinformatic analyses were used to optimize specificity and efficiency, and the efficacy of RNA interference was confirmed by RT-qPCR and Western Blot analysis. siRNA-2 demonstrated the greatest efficacy in reducing VDR expression (Supplementary Material 1 Fig. S1) and was selected for further investigation. The transfection protocol involved seeding NPCs in 6-well plates to 60–70% confluence, then incubating the cells for 6 h with a transfection complex comprising 50 nM siRNA, Opti-MEM, and Lipofectamine 2,000 followed by replacing the medium with growth medium and culturing for 72 h. Four experimental groups

were established: control siRNA + Erastin, control siRNA + 1,25$(OH)_2D_3$+Erastin, VDR siRNA + Erastin, and VDR siRNA + 1,25$(OH)_2D_3$+Erastin. Subsequently, GPX4, ROS, MDA, SOD, GSH, SLC7A11, and SLC40A1 concentrations were quantified in NPCs pre-treated with 1,25$(OH)_2D_3$, both before and after siRNA interference.

Statistical analysis

Data were analyzed using SPSS software (version 23.0) and GraphPad Prism to ensure analytical robustness and reproducibility. All datasets were first tested for normality using the Shapiro-Wilk test ($p > 0.05$), which confirmed that they followed a normal distribution. Based on these results, we used Student's t test for pairwise comparisons and one-way ANOVA with Tukey's post-hoc test for multiple group comparisons, contingent upon the data's distribution. In cases where data did not meet the normality assumption (although in our study all datasets passed the normality test), non-parametric methods would have been applied. All results are expressed as the mean ± standard deviation (SD), and statistical significance was defined as $P < 0.05$, with significance levels indicated as $^{*}P < 0.05$, $^{**}P < 0.01$, and $^{***}P < 0.001$.

Results

Effect of 1,25$(OH)_2D_3$ on the viability of NPCs

The results revealed that NPCs exhibited optimal survivability at 48 h following exposure to a concentration of 10 nmol/L of 1,25$(OH)_2D_3$ (Supplementary Material 1 Fig. S2). This indicates that 1,25$(OH)_2D_3$ can enhance NPC proliferation, with the optimal dose and duration being 10 nmol/L and 48 h, respectively. The selected circumstances were established for the ensuing experiments.

Impact of 1,25$(OH)_2D_3$ on the viability of NPCs treated with Erastin

Microscopic investigation revealed that NPCs in the Erastin group exhibited spindle-shaped, fusiform, and irregular morphologies, marked by sparse distribution and indications of cellular apoptosis. Conversely, the 1,25$(OH)_2D_3$+Erastin group exhibited considerable enhancements in cell proliferation, mirroring the attributes of normal NPCs observed in the control group (Fig. 1). NPCs were pre-treated with 10 nmol/L 1,25$(OH)_2D_3$ for 48 h prior to exposure to 10 µmol/L Erastin for 24 h. This treatment sequence significantly enhanced cell viability (increasing from 0.45 ± 0.09 to 0.67 ± 0.06, $^{***}P < 0.001$) (Fig. 2a) and markedly reduced LDH activity (from 646.46 ± 70.71 U/L to 350.17 ± 30.86 U/L, $^{***}P < 0.001$) (Fig. 2b). These results clearly indicate that pre-treatment with 1,25$(OH)_2D_3$ confers a protective effect against Erastin-induced ferroptosis in NPCs.

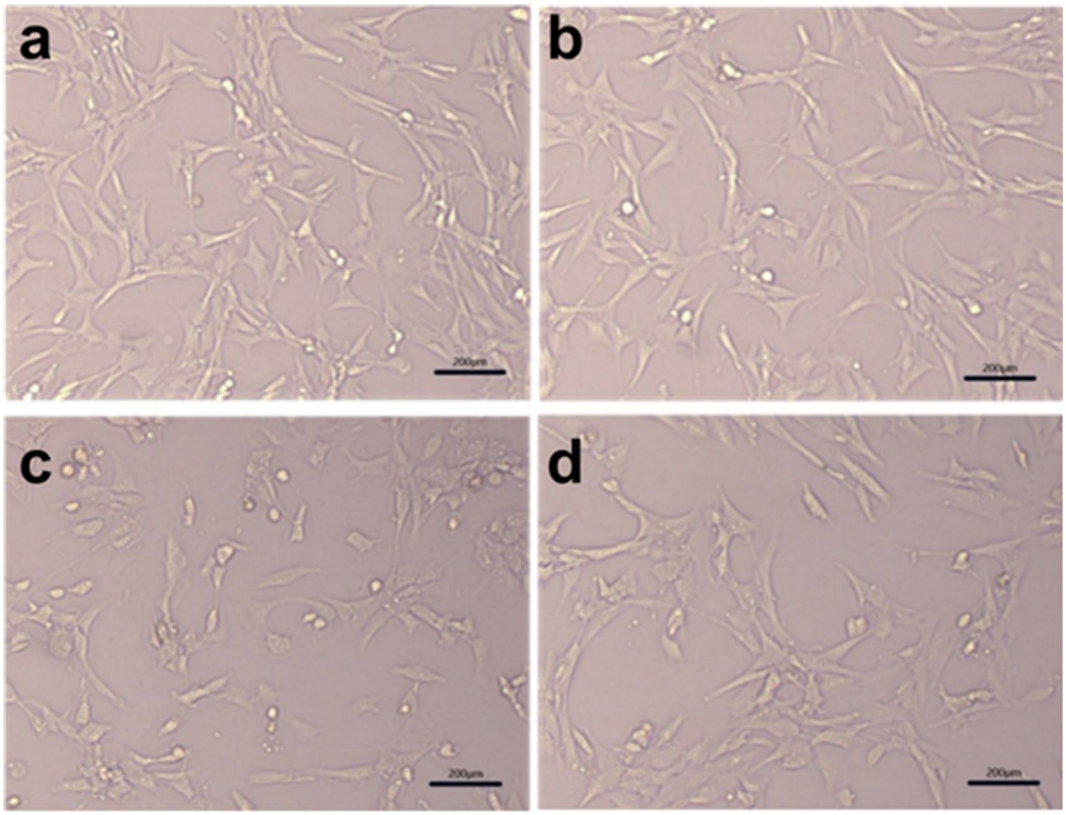

Fig. 1. Microscopic comparison of cell number and growth conditions in experimental and control groups. (**a**) Cell morphology in the blank control group. (**b**) Cell morphology in the 1,25$(OH)_2D_3$ treated group. (**c**) Cell morphology in the Erastin-treated group. (**d**) Cell morphology in the 1,25$(OH)_2D_3$ and Erastin-treated group.

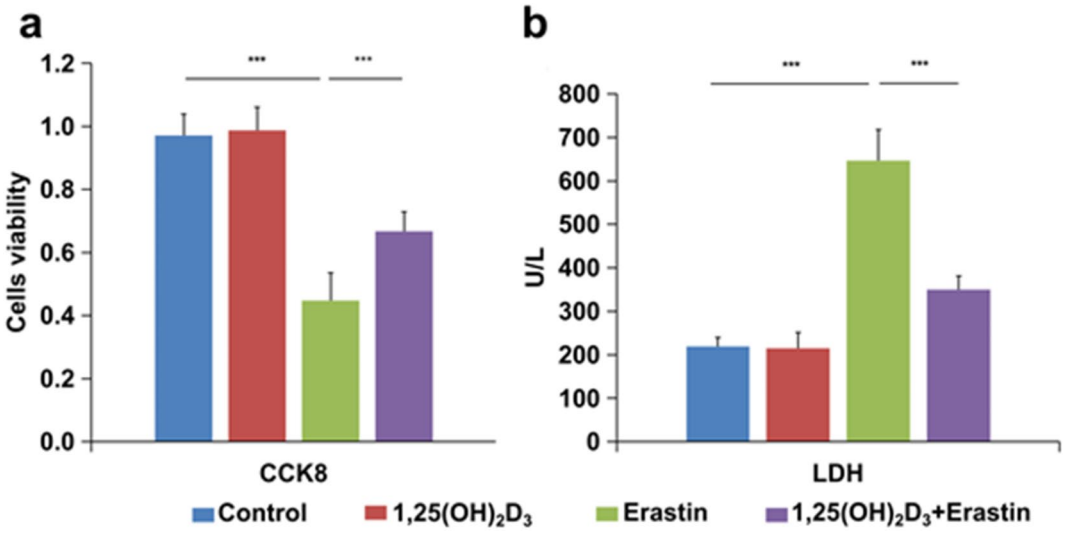

Fig. 2. Enhancement of NPCs proliferation by $1,25(OH)_2D_3$ under ferroptotic conditions. (**a**) Cell viability assessed by CCK8 assay across different groups. (**b**) LDH activity measured by assay kit. The data are presented as the mean ± SD, $^{***}P < 0.001$. $n = 3$.

Effect of $1,25(OH)_2D_3$ on ferroptosis in NPCs

The study investigated the potential of $1,25(OH)_2D_3$ to alleviate ferroptosis in NPCs by measuring intracellular concentrations of GPX4, ROS, MDA, SOD, and GSH in NPCs exposed to Erastin and subsequently treated with $1,25(OH)_2D_3$. The results demonstrated that pretreatment with $1,25(OH)_2D_3$ significantly elevated GPX4 (mRNA relative signal intensity increased from 0.24 ± 0.04 to 0.75 ± 0.05) (Fig. 3a), protein relative signal intensity increased from 0.19 ± 0.02 to 0.42 ± 0.04, $^{***}P < 0.001$), SOD (activity level increased from 54.94 ± 20.33 U/mgprot to 113.92 ± 12.73 U/mgprot, $^{**}P < 0.01$), and GSH (activity level increased from 1.01 ± 0.39 μmol/gprot to 13.99 ± 2.82 μmol/gprot, $^{**}P < 0.01$) levels (Figs. 3b-c and 4b-c), while substantially decreasing ROS (mean fluorescence intensity reduced from 6,555.67 ± 1385.86 to 3,465.67 ± 10.69, $^{**}P < 0.01$) and MDA (activity level decreased from 15.41 ± 2.33 nmol/mgprot to 6.59 ± 2.07 nmol/mgprot, $^{***}P < 0.001$) levels (Fig. 4a and d) in NPCs compared to the Erastin group, indicating diminished oxidative stress in cells treated with $1,25(OH)_2D_3$. This indicates a decrease in oxidative stress in cells treated with $1,25(OH)_2D_3$. RT-qPCR results demonstrated that, relative to the Erastin group, the $1,25(OH)_2D_3$+Erastin group showed a significant elevation in the expression levels of SLC7A11 (mRNA relative signal intensity increased from 0.30 ± 0.03 to 0.55 ± 0.03, $^{*}P < 0.05$) and SLC40A1 (mRNA relative signal intensity increased from 0.23 ± 0.02 to 0.46 ± 0.05, $^{**}P < 0.01$) (Fig. 4e-f). Additionally, transmission electron microscopy analysis of mitochondrial morphology in NPCs indicated that the Erastin group displayed enhanced mitochondrial membrane density and reduced cristae. The mitochondrial morphology in the $1,25(OH)_2D_3$+Erastin group resembled that of the blank control group and the $1,25(OH)_2D_3$ group (Fig. 5). In conclusion, $1,25(OH)_2D_3$ can mitigate ferroptosis in NPCs under ferroptotic circumstances.

Influence of $1,25(OH)_2D_3$ on VDR expression in NPCs

RT-qPCR results demonstrated a significant elevation of VDR in the $1,25(OH)_2D_3$-treated group relative to the control, while VDR was substantially diminished in the Erastin-treated group (mRNA relative signal intensity increased from 0.38 ± 0.07 to 0.77 ± 0.06, Protein relative signal intensity increased from 0.09 ± 0.02 to 0.30 ± 0.02, $^{**}P < 0.01$) (Fig. 6a-b). NPCs pre-treated with $1,25(OH)_2D_3$ demonstrated a significant enhancement in VDR protein expression relative to untreated cells (Fig. 6b), underscoring a possible mechanism through VDR activation. Western Blot examination confirmed these findings, revealing a marked reduction in VDR protein expression in NPCs under ferroptotic conditions, which was reinstated by $1,25(OH)_2D_3$ treatment (Fig. 6c). The findings indicate that VDR activation is essential for the suppression of ferroptosis in NPCs mediated by $1,25(OH)_2D_3$.

Effect of $1,25(OH)_2D_3$ on ferroptosis in NPCs induced by Erastin following VDR gene Silencing

The data indicated that, compared to the VDR siRNA + Erastin group, the VDR siRNA + $1,25(OH)_2D_3$+Erastin group had elevated expression of GPX4 (mRNA relative signal intensity increased from 0.68 ± 0.05 to 1.09 ± 0.06, $^{*}P < 0.05$ Protein relative signal intensity increased from 0.12 ± 0.04 to 0.32 ± 0.08, $^{**}P < 0.01$), SLC7A11 (mRNA relative signal intensity increased from 0.48 ± 0.04 to 1.11 ± 0.18, $^{***}P < 0.001$), SLC40A1 (mRNA relative signal intensity increased from 0.51 ± 0.05 to 1.44 ± 0.13, $^{***}P < 0.001$), SOD (activity level increased from 31.82 ± 8.95 U/mgprot to 42.89 ± 11.93 U/mgprot, $^{**}P < 0.01$) and GSH (activity level increased from 0.70 ± 0.12 μmol/gprot to 9.27 ± 2.45 μmol/gprot, $^{**}P < 0.01$) (Figs. 7 and 8b-c and e-f), alongside a significant reduction in ROS (mean fluorescence intensity decreased from 13,136.33 ± 411.10 to 7,144.33 ± 112.83, $^{***}P < 0.001$) and MDA (activity level decreased from 21.98 ± 2.09 nmol/mgprot to 13.35 ± 3.05 nmol/mgprot, $^{**}P < 0.01$) (Fig. 8a and d). This indicates that $1,25(OH)_2D_3$ continues to exert its inhibitory effect on NPC ferroptosis, even in

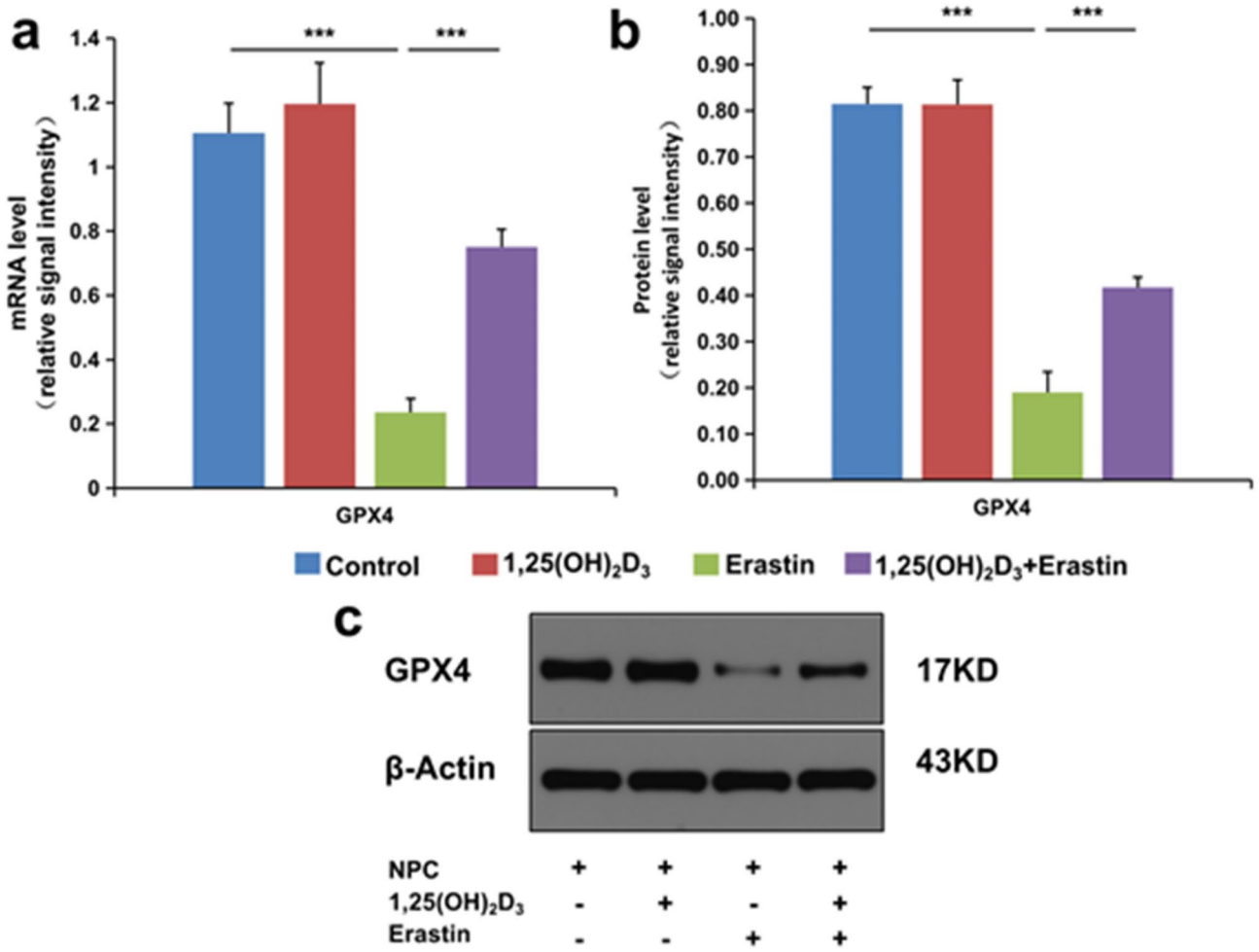

Fig. 3. Augmentation of GPX4 expression in NPCs by $1,25(OH)_2D_3$ under ferroptotic conditions. (**a**) GPX4 expression levels evaluated by RT-qPCR. (**b**) Western Blot quantification of GXP4 protein levels. (**c**) Representative Western Blot images. The data are presented as the mean ± SD, $^{***}P < 0.001$. $n = 3$.

the context of VDR gene suppression. Relative to the control siRNA + $1,25(OH)_2D_3$+Erastin group, the VDR siRNA + $1,25(OH)_2D_3$+Erastin group demonstrated significant reductions in GPX4, SLC7A11, SLC40A1, SOD, and GSH, accompanied by increased levels of ROS and MDA. This indicates that VDR gene silencing diminishes the inhibitory effect of $1,25(OH)_2D_3$ on NPC ferroptosis. The findings confirm that the anti-ferroptotic effect of $1,25(OH)_2D_3$ in NPCs is partially dependent on VDR activation.

Discussion

The development and advancement of LIDD are affected by factors including oxidative stress, trauma, infection and inflammation[30,31]. Oxidative stress is pivotal in the aging of NPCs, resulting in premature senescence due to DNA damage and telomere shortening[32,33]. As degeneration progresses, concentrations of lipid reactive oxygen species, such as superoxide anion, hydroxyl radical, hydrogen peroxide, and nitric oxide, significantly elevate[34,35]. Increased ROS levels expedite LIDD progression through critical signaling pathways, including MAPK and NF-κB. Oxidative stress diminishes the expression of iron transport proteins, resulting in intracellular iron accumulation, which promotes ferroptosis in NPCs and exacerbates LIDD[36]. Homocysteine also enhances GPX4 methylation, thereby associating oxidative stress-induced ferroptosis with LIDD[14]. The findings indicate that alleviating NPC ferroptosis may be a new strategy for avoiding intervertebral disc degeneration.

Our research indicates that $1,25(OH)_2D_3$ markedly promotes NPC proliferation, with an optimal dosage of 10 nmol/L. The cytoprotective properties of $1,25(OH)_2D_3$ seem to be dose-dependent, since elevated doses may diminish its effectiveness. Inadequate levels of $1,25(OH)_2D_3$ impede matrix protein synthesis and expedite disc degeneration, partly due to reduced SIRT1 expression. The activation of SIRT1 by $1,25(OH)_2D_3$ can alleviate degeneration, hence lowering inflammation, oxidative stress, apoptosis, and cellular senescence in intervertebral discs[37]. These findings highlight the therapeutic potential of $1,25(OH)_2D_3$ in the management of disc degeneration.

Erastin, a ferroptosis inducer, reduces levels of GPX4, SOD, and GSH while increasing ROS and MDA, hence facilitating ferroptosis in NPCs. Treatment with $1,25(OH)_2D_3$ promotes NPC growth, viability, and proliferation

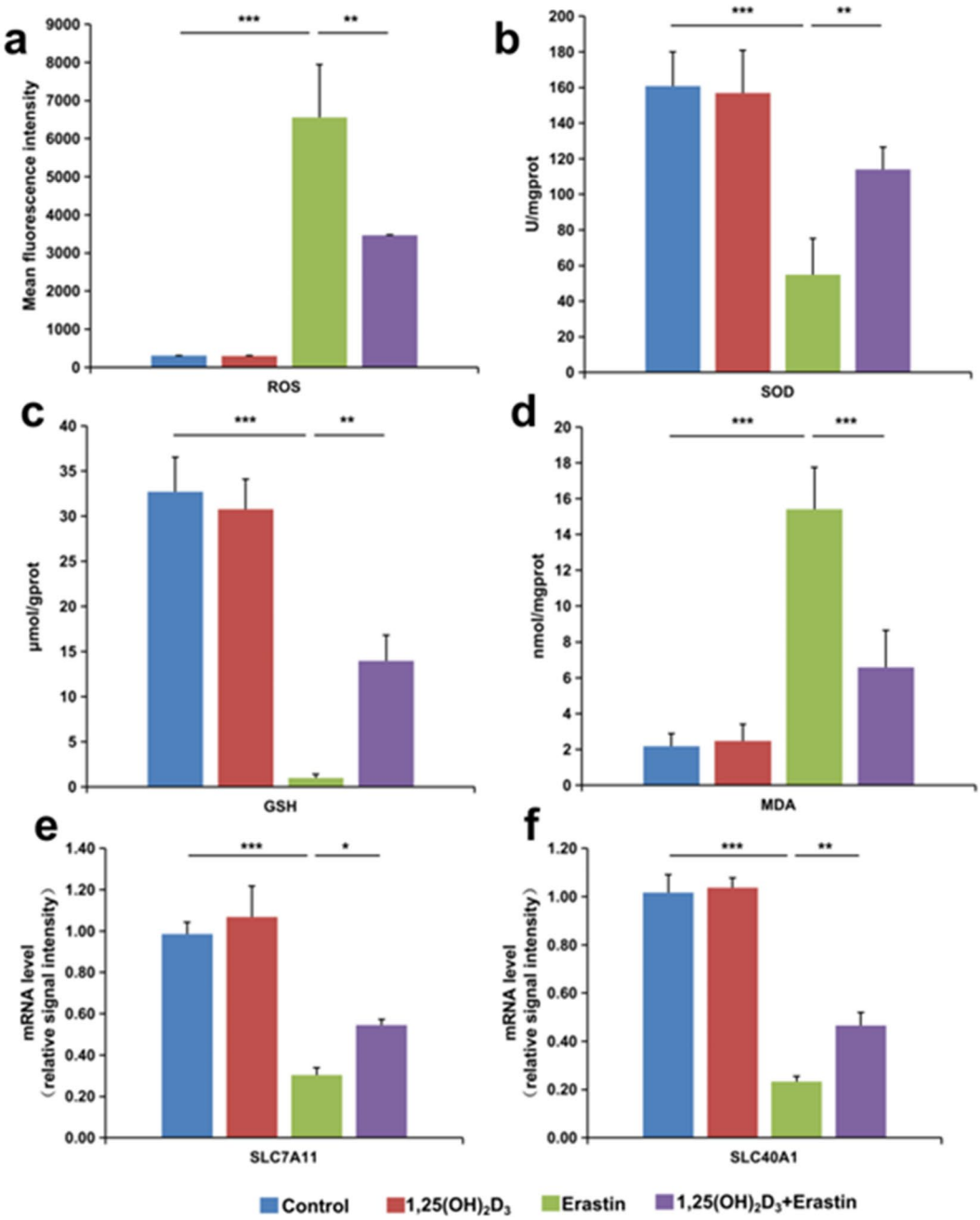

Fig. 4. Effects of $1,25(OH)_2D_3$ on alleviating intracellular oxidative stress and regulating ferroptosis-related gene expression in ferroptotic environment. (**a**) Flow cytometry analysis of intracellular ROS levels. (**b**) Intracellular SOD levels measured using an assay kit. (**c**) Intracellular GSH levels measured using an assay kit. (**d**) Intracellular MDA levels measured using an assay kit. (**e**) Relative mRNA expression levels of SLC7A11 analyzed by RT-qPCR. (**f**) Relative mRNA expression levels of SLC40A1 analyzed by RT-qPCR. The data are presented as the mean ± SD, $^{**}P < 0.01$, $^{***}P < 0.001$. $n = 3$.

in ferroptotic circumstances, elevating GPX4, SOD, and GSH levels while diminishing ROS and MDA. Proteins including SLC7A11 and SLC40A1, which are crucial regulators of ferroptosis, exhibit increased expression in NPCs exposed to $1,25(OH)_2D_3$, hence alleviating oxidative stress and iron buildup. Furthermore, mitochondrial modifications, characteristic of ferroptosis, were mitigated by $1,25(OH)_2D_3$, as demonstrated by TEM data indicating restored mitochondrial shape and reduced cristae damage. These findings align with prior studies that highlight the pivotal role of mitochondrial integrity in ferroptosis regulation. However, while our study emphasizes mitochondrial morphology as a key indicator, functional assessments such as ATP production and oxygen consumption rates would provide more robust evidence to confirm the protective role of $1,25(OH)_2D_3$ in ferroptosis. Future studies should aim to integrate these functional assays to strengthen the mechanistic

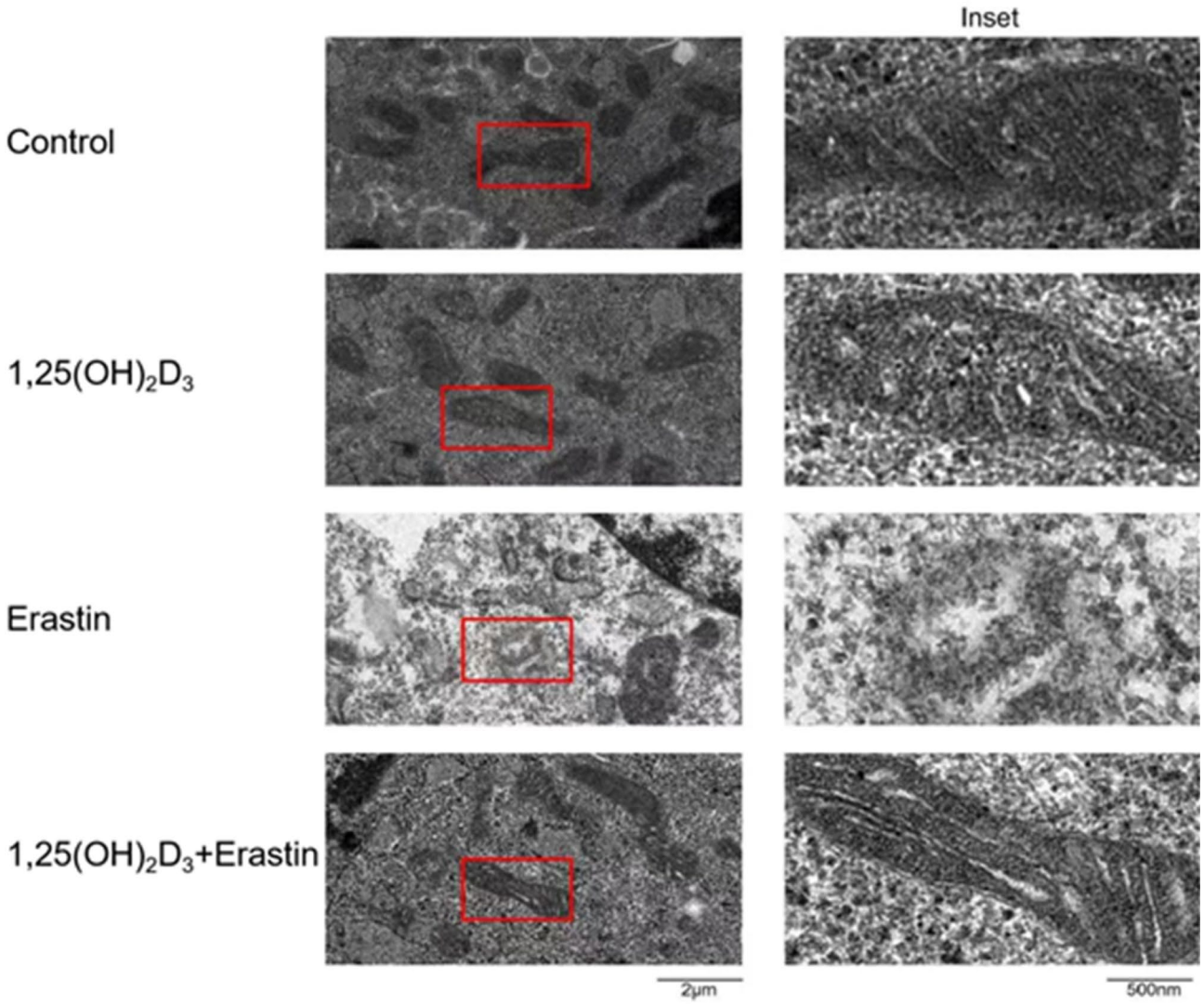

Fig. 5. Transmission electron microscopy observation of mitochondrial morphology in NPCs. The mitochondrial membrane density increased and cristae reduced in the Erastin group, whereas the $1,25(OH)_2D_3$+Erastin group exhibited characteristics similar to the control and $1,25(OH)_2D_3$ group.

understanding of $1,25(OH)_2D_3$ mediated ferroptosis alleviation. The findings indicate that $1,25(OH)_2D_3$ efficiently safeguards NPCs from ferroptosis by regulating oxidative stress and mitochondrial integrity.

GPX4, SLC7A11, and SLC40A1, identified as indicators of ferroptosis, are crucial in situations including cancer, neurodegeneration, and ischemia-reperfusion injury[38]. GPX4 inhibits apoptosis by diminishing lipid peroxidation, whereas SLC7A11 and SLC40A1 modulate antioxidant defenses and iron metabolism, respectively. Modifications in the expression of these proteins can trigger ferroptosis, creating avenues for therapeutic intervention[39,40]. Modulating these biomarkers presents diagnostic and therapeutic possibilities for ferroptosis-related disorders, warranting additional research.

The VDR, a nuclear receptor that regulates transcription and calcium transport[41], is crucial in reducing ferroptosis in NPCs. In ferroptotic circumstances, VDR expression diminishes. However, treatment with $1,25(OH)_2D_3$ reinstates its levels, indicating that VDR activation is essential for the protective effects of $1,25(OH)_2D_3$. This protection entails the inhibition of autophagy and oxidative stress via pathways including mTOR/p70S6k[18] and PINK1/Parkin[42]. siRNA-induced VDR knockdown reduces the protective effects of $1,25(OH)_2D_3$, highlighting VDR's critical function in NPC survival and the prevention of ferroptosis. Although there is limited effectiveness in VDR-silenced environments, the results underscore the intricate relationship between $1,25(OH)_2D_3$ and VDR in addressing oxidative stress and ferroptosis.

These findings suggest that targeting VDR with $1,25(OH)_2D_3$ may be clinically significant in the management of LIDD. The capacity of $1,25(OH)_2D_3$ to improve NPC viability and inhibit ferroptosis underscores its promise as a therapeutic agent. Future clinical methods may investigate the application of $1,25(OH)_2D_3$ or its analogs in conjunction with other therapies to avert or mitigate the advancement of intervertebral disc degeneration. Clinical trials assessing the safety, appropriate dosage, and long-term efficacy of $1,25(OH)_2D_3$ in patients with

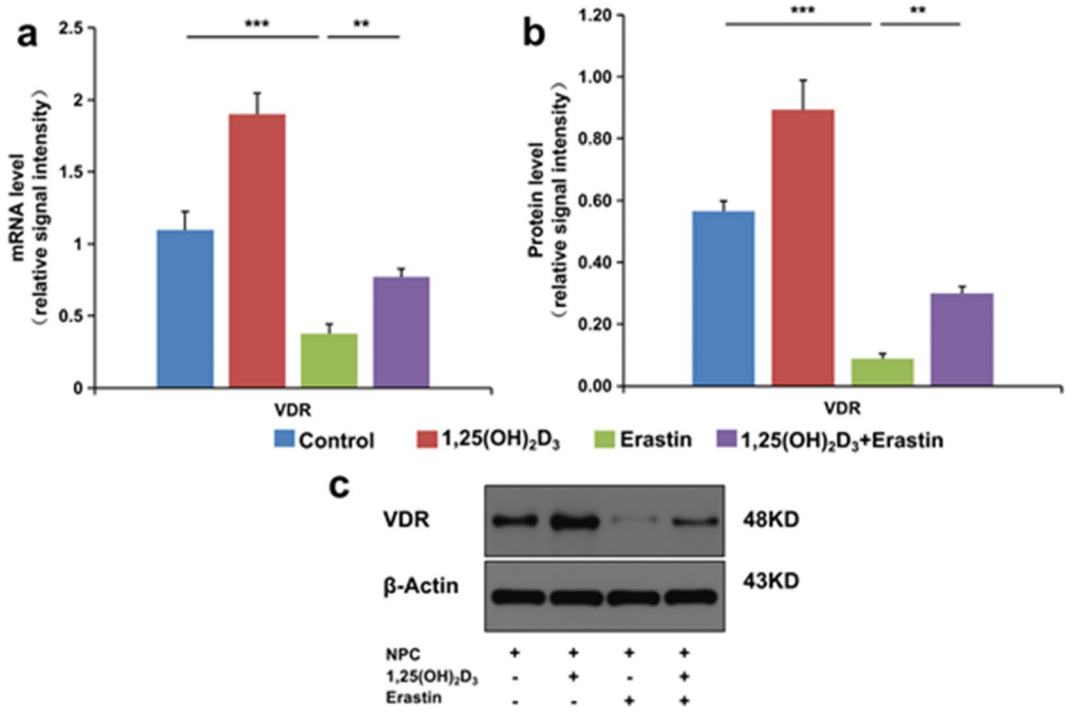

Fig. 6. Restoration of VDR expression by $1,25(OH)_2D_3$ in ferroptotic environment. (**a**) RT-qPCR analysis of VDR expression. (**b**) Western Blot quantification of VDR protein levels. (**c**) Representative Western Blot images. The data are presented as the mean ± SD, $^{**}P < 0.01$, $^{***}P < 0.001$. $n = 3$.

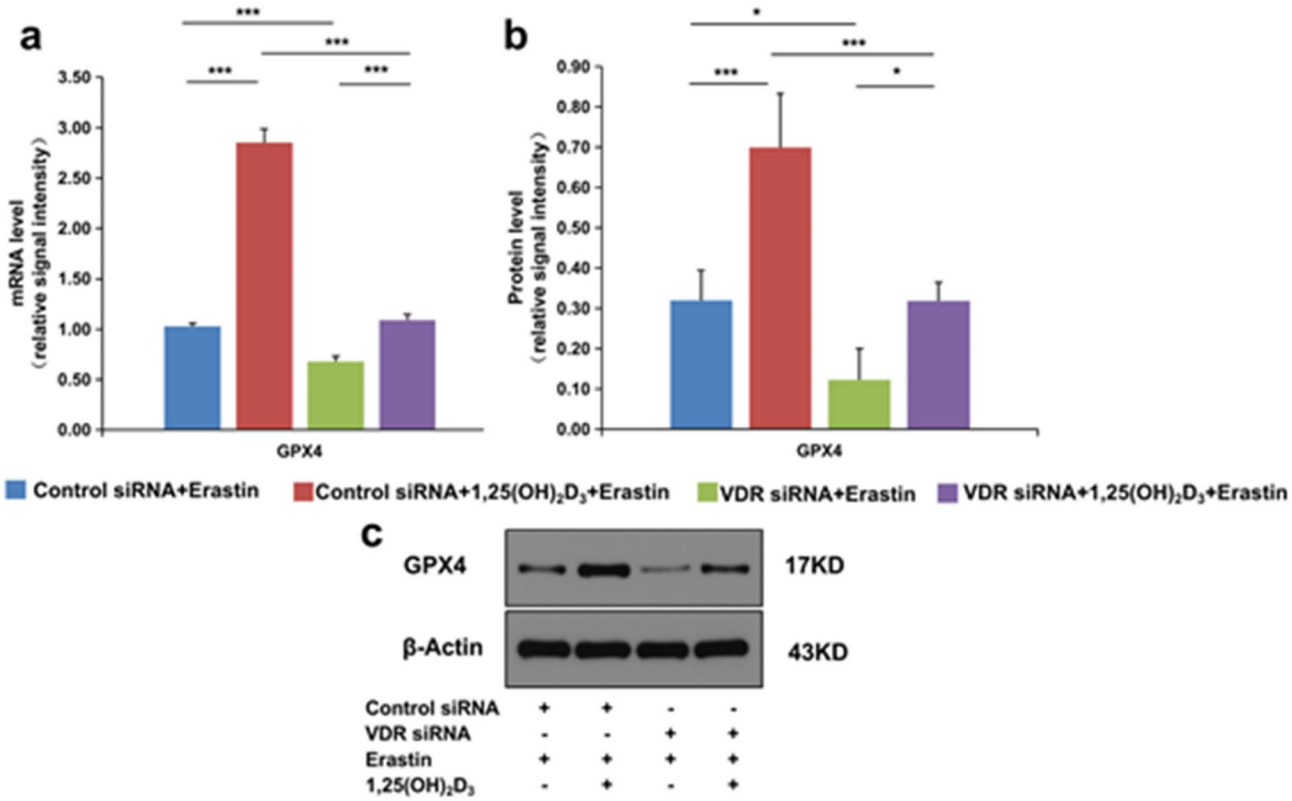

Fig. 7. $1,25(OH)_2D_3$ potentially increases intracellular GPX4 expression partially through VDR activation. (**a**) RT-qPCR analysis of GPX4 expression. (**b**) Western Blot quantification of GXP4 protein levels. (**c**) Representative Western Blot images. The data are presented as the mean ± SD, $^{*}P < 0.05$, $^{***}P < 0.001$. $n = 3$.

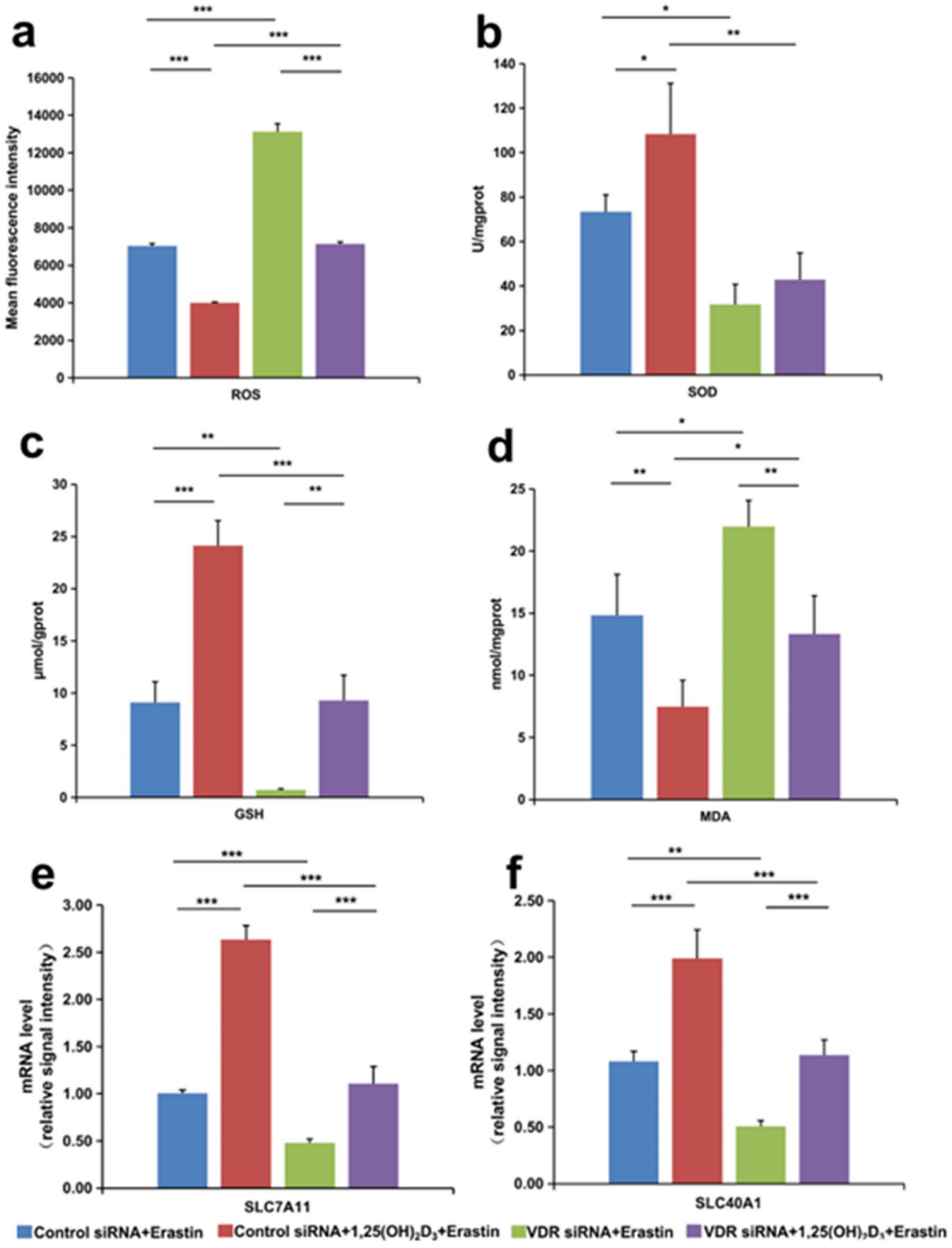

Fig. 8. Effects of $1,25(OH)_2D_3$ on alleviating intracellular oxidative stress and regulating ferroptosis-related gene expression in ferroptotic environment. (**a**) Flow cytometry analysis of intracellular ROS levels. (**b**) Intracellular SOD levels measured using an assay kit. (**c**) Intracellular GSH levels measured using an assay kit. (**d**) Intracellular MDA levels measured using an assay kit. (**e**) Relative mRNA expression levels of SLC7A11 analyzed by RT-qPCR. (**f**) Relative mRNA expression levels of SLC40A1 analyzed by RT-qPCR. The data are presented as the mean ± SD, $^{**}P < 0.01$, $^{***}P < 0.001$. $n = 3$.

LIDD will be crucial for turning these findings into therapeutic applications. This discovery highlights the necessity of further exploring the VDR-mediated pathways and its ramifications for the development of targeted treatments for intervertebral disc degeneration.

Conclusions

In conclusion, this study effectively established the optimal conditions under which $1,25(OH)_2D_3$ enhances the proliferation of rat NPCs. Utilizing Erastin to mimic ferroptosis conditions, it was demonstrated that

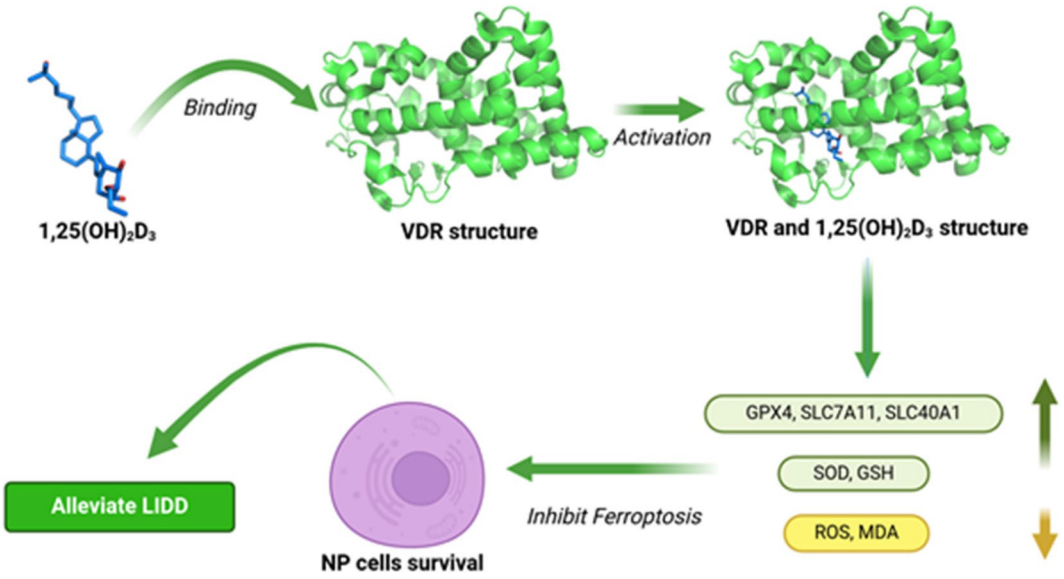

Fig. 9. $1,25(OH)_2D_3$ directly interacts with VDR (PDBID: 2HAS), thereby activating it to enhance the expression of ferroptosis protective proteins and antioxidants while diminishing indicators of oxidative stress, finally reducing ferroptosis in NPCs and alleviating LIDD.

$1,25(OH)_2D_3$ reduces ferroptosis in NPCs by upregulating ferroptosis protective proteins and antioxidants while decreasing oxidative stress markers. Notably, a reduction in VDR expression was observed under ferroptotic conditions. The subsequent VDR gene silencing experiments revealed that while $1,25(OH)_2D_3$ continues to mitigate ferroptosis, its efficacy is diminished without VDR activation, highlighting the significance of VDR in its protective mechanism (Fig. 9). This opens avenues for further exploration into additional pathways by which $1,25(OH)_2D_3$ may exert its therapeutic effects.

Data availability

The data supporting the study results are available from the corresponding author upon reasonable request.

Received: 10 December 2024; Accepted: 27 February 2025
Published online: 07 March 2025

References

1. Maher, C., Underwood, M. & Buchbinder, R. Non-specific low back pain. *Lancet* **389**, 736–747 (2017).
2. Knezevic, N. N., Candido, K. D., Vlaeyen, J. W. S., Zundert, J. & Cohen, S. P. Low back pain. *Lancet* **398**, 78–92 (2021).
3. Cao, C. et al. Bone marrow mesenchymal stem cells slow intervertebral disc degeneration through the NF-κB pathway. *Spine J.* **15**, 530–538 (2015).
4. Millecamps, M. & Stone, L. S. Delayed onset of persistent discogenic axial and radiating pain after a single-level lumbar intervertebral disc injury in mice. *Pain* **159**, 1843–1855 (2018).
5. Liu, J., Yu, J., Jiang, W., He, M. & Zhao, J. Targeting of CDKN1B by miR-222-3p May contribute to the development of intervertebral disc degeneration. *FEBS Open. Bio.* **9**, 728–735 (2019).
6. Binch, A. L. A., Fitzgerald, J. C., Growney, E. A. & Barry, F. Cell-based strategies for IVD repair: clinical progress and translational Obstacles. *Nat. Rev. Rheumatol.* **17**, 158–175 (2021).
7. Dou, X. et al. Therapeutic potential of melatonin in the intervertebral disc degeneration through inhibiting the ferroptosis of nucleus pulpous cells. *J. Cell. Mol. Med.* **27**, 2340–2353 (2023).
8. Zhao, C. Q., Wang, L. M., Jiang, L. S. & Dai, L. Y. The cell biology of intervertebral disc aging and degeneration. *Ageing Res. Rev.* **6**, 247–261 (2007).
9. Fan, C. et al. The role of ferroptosis in intervertebral disc degeneration. *Front. Cell. Dev. Biol.* **11**, (2023).
10. Zhang, L. et al. Insight into the Double-Edged Role of Ferroptosis in Disease. *Biomolecules* 11, (2021).
11. Dixon, S. J. et al. Ferroptosis: an iron-dependent form of nonapoptotic cell death. *Cell* **149**, 1060–1072 (2012).
12. Stockwell, B. R. et al. Ferroptosis: A regulated cell death Nexus linking metabolism, redox biology, and disease. *Cell* **171**, 273–285 (2017).
13. Xiong, Y. et al. The Regulatory Role of Ferroptosis in Bone Homeostasis. *Stem Cells Int* (2022). (2022).
14. Zhang, X. et al. Homocysteine induces oxidative stress and ferroptosis of nucleus pulposus via enhancing methylation of GPX4. *Free Radic Biol. Med.* **160**, 552–565 (2020).
15. Yang, R. Z. et al. Involvement of oxidative stress-induced annulus fibrosus cell and nucleus pulposus cell ferroptosis in intervertebral disc degeneration pathogenesis. *J. Cell. Physiol.* **236**, 2725–2739 (2021).
16. Misof, B. M. et al. No role of osteocytic osteolysis in the development and recovery of the bone phenotype induced by severe secondary hyperparathyroidism in vitamin D receptor deficient mice. *Int. J. Mol. Sci.* **21**, (2020).
17. Rosen, C. J. et al. The nonskeletal effects of vitamin D: an endocrine society scientific statement. *Endocr. Rev.* **33**, 456–492 (2012).
18. Tong, T. et al. Age-dependent expression of the vitamin D receptor and the protective effect of vitamin D receptor activation on H(2)O(2)-induced apoptosis in rat intervertebral disc cells. *J. Steroid Biochem. Mol. Biol.* **190**, 126–138 (2019).
19. Dong, J. et al. Calcitriol protects renovascular function in hypertension by down-regulating angiotensin II type 1 receptors and reducing oxidative stress. *Eur. Heart J.* **33**, 2980–2990 (2012).

20. Withanage, N. D., Perera, S., Peiris, H. & Athiththan, L. V. Serum 25-hydroxyvitamin D, serum calcium and vitamin D receptor (VDR) polymorphisms in a selected population with lumbar disc herniation-A case control study. *PLoS One* **13**, (2018).
21. Xu, H. W. et al. Does vitamin D status influence lumbar disc degeneration and low back pain in postmenopausal women? A retrospective single-center study. *Menopause* **27**, 586–592 (2020).
22. Krasowska, K. et al. The preoperative supplementation with vitamin D attenuated pain intensity and reduced the level of Pro-inflammatory markers in patients after posterior lumbar interbody fusion. *Front. Pharmacol.* **10**, (2019).
23. Zhang, C., Tong, T., Miao, D. C. & Wang, L. F. Vitamin D inhibits TNF-α induced apoptosis of human nucleus pulposus cells through regulation of NF-kB signaling pathway. *J. Orthop. Surg. Res.* **16**, (2021).
24. Videman, T. et al. Determinants of the progression in lumbar degeneration: a 5-year follow-up study of adult male monozygotic twins. *Spine* **31**, 671–678 (2006).
25. Biczo, A., Szita, J., McCall, I., Varga, P. P. & Lazary, A. Association of vitamin D receptor gene polymorphisms with disc degeneration. *Eur. Spine J.* **29**, 596–604 (2020).
26. Pękala, P. A. et al. Vitamin D receptor gene polymorphism influence on lumbar intervertebral disc degeneration. *Clin. Anat.* **35**, 738–744 (2022).
27. Li, Z. et al. Notch3 regulates ferroptosis via ROS-induced lipid peroxidation in NSCLC cells. *FEBS Open. Bio.* **12**, 1197–1205 (2022).
28. Bikle, D. D., Vitamin, D. & Metabolism Mechanism of action, and clinical applications. *Chem. Biol.* **21**, 319–329 (2014).
29. Hu, Z. et al. VDR activation attenuate cisplatin induced AKI by inhibiting ferroptosis. *Cell. Death Dis.* **11**, 73 (2020).
30. Vo, N. et al. An overview of underlying causes and animal models for the study of age-related degenerative disorders of the spine and synovial joints. *J. Orthop. Res.* **31**, 831–837 (2013).
31. Feng, C. et al. Disc cell senescence in intervertebral disc degeneration: causes and molecular pathways. *Cell. Cycle.* **15**, 1674–1684 (2016).
32. Cheng, F. et al. The role of oxidative stress in intervertebral disc cellular senescence. *Front. Endocrinol. (Lausanne* **13**, (2022).
33. Wen, P. et al. The role of ageing and oxidative stress in intervertebral disc degeneration. *Front. Mol. Biosci.* **9**, (2022).
34. Valgimigli, L. Lipid peroxidation and antioxidant protection. *Biomolecules* **13**, (2023).
35. Wang, Y. et al. Oxidative stress in intervertebral disc degeneration: molecular mechanisms, pathogenesis and treatment. *Cell. Prolif.* **56**, (2023).
36. Lu, S. et al. Ferroportin-Dependent Iron Homeostasis Protects against Oxidative Stress-Induced Nucleus Pulposus Cell Ferroptosis and Ameliorates Intervertebral Disc Degeneration In Vivo. *Oxid Med Cell Longev* (2021). (2021).
37. Huang, H. et al. Vitamin D retards intervertebral disc degeneration through inactivation of the NF-κB pathway in mice. *Am. J. Transl Res.* **11**, 2496–2506 (2019).
38. Jiang, X., Stockwell, B. R. & Conrad, M. Ferroptosis: mechanisms, biology and role in disease. *Nat. Rev. Mol. Cell. Biol.* **22**, 266–282 (2021).
39. Janssen, E. M. et al. Analysis of patient preferences in lung Cancer - Estimating acceptable tradeoffs between treatment benefit and side effects. *Patient Prefer Adherence.* **14**, 927–937 (2020).
40. Hao, L. et al. SLC40A1 mediates ferroptosis and cognitive dysfunction in type 1 diabetes. *Neuroscience* **463**, 216–226 (2021).
41. Bikle, D. D. Vitamin D metabolism, mechanism of action, and clinical applications. *Chem. Biol.* **21**, 319–329 (2014).
42. Lan, T., Yan, B., Guo, W., Shen, Z. & Chen, J. VDR promotes nucleus pulposus cell mitophagy as a protective mechanism against oxidative stress injury. *Free Radic Res.* **56**, 316–327 (2022).

Author contributions

LQ contributed to project design, performed the experiments and wrote the manuscript. PJ contributed to the experiments, collected analysis data, and wrote the manuscript. DF reviewed the manuscript and provided financial support. All authors read and approved the final manuscript.

Funding

This research has been supported by the National Natural Science Foundation of China (Grant No.: 81601943), and the China Hubei Provincial Health Commission Research Project (Grant No.: WJ2019M023).

Declarations

Competing interests

The authors declare no competing interests.

Additional information

Supplementary Information The online version contains supplementary material available at https://doi.org/10.1038/s41598-025-92405-x.

Correspondence and requests for materials should be addressed to F.D.